ACS Catalysis

Research Article

pubs.acs.org/acscatalysis

High-Pressure Adsorption of Ethylene on Cubic Pt Nanoparticles and Pt(100) Single Crystals Probed by in Situ Sum Frequency Generation Vibrational Spectroscopy

S. J. Kweskin,[†,‡,∥] R. M. Rioux,*[,†,‡,⊥] H. Song,[†,‡,⊗] K. Komvopoulos,[§] P. Yang,[†,‡] and G. A. Somorjai*[,†,‡]

[†]Department of Chemistry and [§]Department of Mechanical Engineering, University of California, Berkeley, California 94720, United States

[‡]Materials Sciences Division, Lawrence Berkeley National Laboratory, Berkeley, California 94720, United States

ABSTRACT: A model catalytic system of a monolayer consisting of 9-nm average size, cubic, single-crystal Pt nanoparticles and poly(vinylpyrrolidone) (PVP) polymer capping agent deposited on a sapphire prism was investigated by sum-frequency generation (SFG) vibrational spectroscopy in total internal reflection (TIR) geometry. Exposure of a clean nanoparticle monolayer after removal of PVP by cyclic oxidation−reduction treatment to high-pressure ethylene at room temperature led to the formation of ethylidyne and di-σ bonded ethylene. Low-pressure ethylene adsorption on a pseudohexagonal reconstructed Pt(100) single crystal resulted only in the formation of di-σ bonded ethylene. High-pressure adsorption of ethylene on Pt nanoparticle monolayers and Pt(100) led to the formation of both ethylidyne and di-σ bonded ethylene and stabilized the pseudohexagonal reconstruction of Pt(100) on both the single crystal and the surface of clean cubic nanoparticles. Restructuring of the PVP layer caused by CO adsorption indicated a small fraction of the Pt surface was available for adsorption. The stretching frequency of linear-bound CO red-shifted relative to CO adsorption on a clean Pt nanoparticle monolayer. PVP reversibly restructured upon the removal of CO by oxidation at room temperature. After the near complete removal of PVP by a cyclic low-temperature oxidation−reduction process, the peak position of the linear-bound CO blue-shifted to a frequency consistent with the adsorption of CO on a clean Pt surface. The successful application of TIR-SFG to catalytically relevant surfaces under high-pressure conditions demonstrated in this study is a significant advance in the detection of surface intermediates.

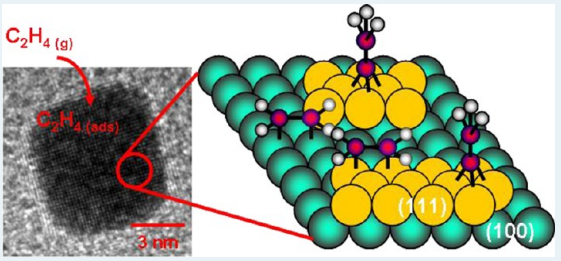

KEYWORDS: *adsorbate-induced reconstruction, carbon monoxide, ethylene, nanoparticles, platinum, single crystals, sum-frequency generation (SFG) vibrational spectroscopy, poly(vinylpyrrolidone)*

1. INTRODUCTION

Molecular-level insight into catalytic reactions occurring under industrially relevant operating conditions is of paramount importance in heterogeneous catalysis.[1] However, basic understanding of catalytic reactions at the molecular scale is challenging because it requires detailed characterization of the surface structure (e.g., facets, steps, and defects) of metal nanocrystals and in situ techniques for probing adsorbate-solid surface interactions under reaction conditions. Although single crystals are model systems of real industrial catalysts, they do not incorporate all of the physical and chemical complexities of industrial catalysts.[2] Furthermore, very few techniques are capable of detecting surface adsorbates under equilibrium conditions in a high-pressure gas atmosphere.[3] The previous challenges are generally referred to as the "materials and pressure gaps" in heterogeneous catalysis.[4] In situ techniques enable surface-specific information for more advanced model systems[5] to be obtained in high-pressure gas environments.[5−7]

Sum frequency generation (SFG) vibrational spectroscopy is a nonlinear spectroscopy technique that can detect adsorbates at catalytically relevant interfaces under high temperatures and pressures. SFG has yielded significant insight into gas−solid interfaces under catalytic conditions.[5,6,8−12] The surface sensitivity of SFG is derived from the fact that SFG photons are produced where centrosymmetry is broken, a natural property of an interface, such as the gas−solid interface of a heterogeneous catalyst. A signal from the bulk is eliminated because the high-pressure gas environment is isotropic and, under the electric dipole approximation,[13] it does not generate SFG photons, making SFG sensitive only to the adsorbate monolayer. This specificity is sensitive down to submonolayer coverage. SFG has been applied primarily to flat (optically smooth) interfaces, such as single crystals.[14] The extension of SFG to optically complex surfaces with micrometer and submicrometer features has been achieved by standard collection techniques,[6,15−17] diffuse reflectance,[18] and total internal reflection (TIR) approaches.[19,20] SFG spectra have

Special Issue: Operando and In Situ Studies of Catalysis

Received: July 29, 2012
Revised: September 30, 2012

   dx.doi.org/10.1021/cs3005067 | *ACS Catal.* 2012, 2, 2377−2386

been obtained during the adsorption and oxidation of CO on Langmuir–Blodgett (LB) monolayers of Pt nanoparticles using TIR geometry.[19] SFG has also been applied to probe alcohol adsorption on silica powder,[20] the adsorption of carbon monoxide on a Al_2O_3-supported catalyst,[21] and to study the catalytic reactivity of metallic nanoparticles during hydrogenation reactions.[22,23]

The objective of this study was to examine if a coherent SFG signal can be obtained from small-probe molecules (i.e., ethylene and CO) adsorbed on monolayers of 9-nm average size, cubic Pt nanoparticles synthesized by colloidal chemistry[24−26] using the TIR-SFG technique at atmospheric pressure. The decomposition and removal of the poly(vinylpyrrolidone) (PVP) polymer template from the monolayer by cyclic oxidation–reduction treatments and the interaction of CO with as-synthesized, clean Pt nanoparticles were examined by in situ TIR-SFG. High-pressure adsorption of ethylene on clean Pt nanoparticles led to the formation of ethylidyne and di-σ bonded ethylene. Similar SFG spectra were obtained for ethylene adsorption on cubic Pt nanoparticles and single-crystal Pt(111) surfaces, suggesting that the Pt nanoparticles stabilized the pseudohexagonal Pt(100) surface when in equilibrium with high-pressure ethylene. Ethylidyne was identified on a pseudohexagonal Pt(100) single crystal only after high-pressure adsorption of ethylene, indicating that ethylidyne stabilized the pseudohexagonal surface. The obtained results reveal that the surface chemistry on small particles is similar to a single-crystal surface, as in the examined cases of ethylene adsorption on clean cubic Pt nanoparticles and Pt(100) single crystal.

2. EXPERIMENTAL PROCEDURES

2.1. Monolayer Synthesis from Platinum Nanoparticles. Cubic Pt nanoparticles with an average size of 9 nm (largest vertex-to-vertex distance) were synthesized by a modified polyol process in the presence of PVP.[27] After heating 2.5 mL of ethylene glycol (EG) at reflux (553 K) for 5 min, 0.5 mL of $AgNO_3$ solution (2 mM, Ag/Pt = 1.1 mol %) was added to the boiling EG, immediately followed by alternating additions of EG solutions of PVP (93.8 μL, 0.375 M) and $H_2PtCl_6{\cdot}6H_2O$ (46.9 μL, 62.5 mM) into the mixture every 30 s over a period of 16 min (i.e., a total of 16 additions of each solution). The resulting solution was refluxed for an additional 5 min. The products consisting of ∼80% cubes were purified by repetitive precipitation and centrifugation and finally dispersed in chloroform.

A chloroform solution of colloidal Pt was dispersed onto a deionized water (18 MΩ·cm resistivity) subphase on a LB trough (type 611, NIMA Technology, Coventry, England) at room temperature. Pt nanoparticles were deposited onto an equilateral sapphire prism (20 mm × 20 mm base, Red Optronics, Mountain View, CA) using a LB trough while monitoring the surface pressure with a Wilhelmy plate. Prior to spreading the particles, the surface pressure was adjusted to zero and the film was compressed by a mobile barrier at a rate of 0.3 cm^2/min. The Pt monolayer at the water/air interface was transferred at a surface pressure of 6 mN/m (40% of a monolayer) onto the surface of an equilateral sapphire prism by the Langmuir–Schäffer horizontal lift-off method[28] and dried in air. This surface pressure corresponds to a 40% surface area coverage of the base of the sapphire prism by nanoparticles or 0.4 ML surface coverage (ML = monolayer).

2.2. Ethylene Adsorption on Pt(100) under Ultrahigh Vacuum and High Pressure Conditions.[29] Single-crystal Pt samples were mounted in an ultrahigh vacuum (UHV), high-pressure reaction chamber, which was pumped down to a base pressure of 2×10^{-10} Torr by turbomolecular and ion pumps. The chamber was equipped with a retarding field analyzer for Auger electron spectroscopy (AES) and low energy electron diffraction (LEED). The sample could be resistively heated to 1200 K and cooled down to 140 K under vacuum with liquid nitrogen. The Pt(100) single crystal was cleaned in vacuum (5×10^{-5} Torr) by repeated cycles of Ar^+ ion bombardment and then heated in O_2 (5×10^{-7} Torr) at ∼1125 K for 2 min. After the removal of the oxygen, the crystal was annealed at 1135 K for 1 min under a pressure of $<2 \times 10^{-9}$ Torr. The surface cleanliness was verified by AES. Adsorption gases were introduced through a gas manifold system evacuated by a turbomolecular pump. Further details of the experimental apparatus can be found in previous publications.[30,31]

SFG spectra were obtained with a Nd:YAG laser system (Leopard, Continuum, Santa Clara, CA). The laser operated at 20 Hz produced 20 ps pulses of fundamental wavelength 1064 nm and energy 35 mJ. The 1064-nm output was passed through an optical parametric generation-amplification (OPG/OPA) system to generate a tunable (1800–4000 cm^{-1}) infrared (IR) beam. A portion of the Nd:YAG fundamental was frequency doubled (λ = 532 nm) and the tunable IR beam was passed through CaF_2 windows into the UHV chamber. Both beams were spatially and temporally overlapped on the single-crystal surface at incident angles of 60° and 65° with respect to the surface normal. SFG photons reflected off the single-crystal surface were guided through a monochromator. The signal intensity was detected by a photomultiplier tube (Hamamatsu, Bridgewater, NJ) and collected with a gated integrator (Stanford Research Systems, Sunnyvale, CA). Details of the laser system and optical setup used in this study can be found elsewhere.[13,30,31]

2.3. Reaction Cell for in Situ Total Internal Reflection-SFG Vibrational Spectroscopy. Figure 1A shows a photograph of the experimental setup used in this study to perform in situ TIR-SFG characterization of adsorbates on ordered nanoparticle monolayers. An equilateral sapphire prism was held in compression against a Viton O-ring (∼17 mm in diameter) by a Teflon block fitted onto the prism apex and secured by two set screws (inset of Figure 1A).[19] A vacuum manifold connected to mechanical and sorption pumps produced a vacuum of ∼10 mTorr in the reaction cell, while a gas manifold equipped with a series of mass flow controllers (Porter Instruments, Hatfield, PA) provided continuous gas flow through the spectroscopy-reactor cell at atmospheric pressure. High-purity H_2 (Praxair, UHP, 99.999%), He (Praxair, UHP, 99.999%), 20% O_2/He mixture (Praxair, UHP, 99.999%), CO (AirGas, CP grade), and C_2H_4 (Praxair, CP grade) were used in their as-received condition. The total flow rate of the reactant gases was 95 cm^3(STP)/min. The temperature was measured by a thermocouple placed in direct contact with the underside of the sapphire prism, while the prism sides were heated with two Kapton resistive elements (Omega Engineering, Stamford, CT). Temperature variations across the base of the prism were found to be less than 2 K.

2.4. In Situ Total Internal Reflection-SFG Vibrational Spectroscopy. Surface spectroscopy of the Pt nanoparticle LB monolayers used the previously described laser setup to generate the tunable IR and 532-nm visible (Vis) beams. A

dx.doi.org/10.1021/cs3005067 | ACS Catal. 2012, 2, 2377−2386

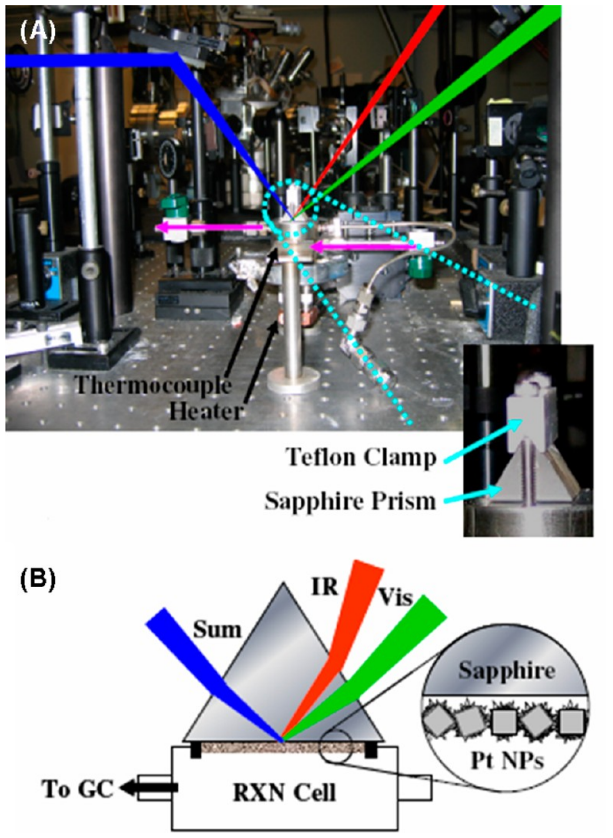

Figure 1. (A) Photograph of SFG spectroscopy-reactor cell for in situ adsorption and reaction studies on Pt nanoparticle monolayers.[19] The small photograph (inset) shows the single-crystal sapphire prism sealed against an O-ring mounted in the reactor body and held in gastight contact by a Teflon clamp and a pair of threaded screws. (The purple arrows indicate the gas flow direction.) (B) Schematic of the total-internal reflection (TIR) setup and the sapphire-nanoparticle interface. PVP-capped Pt nanoparticles (NPs) were deposited onto the single-crystal sapphire prism by a monolayer lift-off technique. The spectroscopy cell operates as a continuous flow reactor. (The gas-manifold and bank of mass flow controllers connected to the manifold are not in the frame of the photograph.).

schematic of the sapphire-nanoparticle interface is shown in Figure 1B. The IR and Vis beams were passed through the sapphire prism at angles greater than the critical angle for TIR and, subsequently, reflected off the sapphire-nanoparticle interface. The SFG signal was collected using the same method as for the single crystal measurements. Because of the complicated nonlinear response of this system caused by scattering interactions, angular effects, polarizability, signal contributions from opposite particle sides,[32] dielectric dispersion,[33] and attenuation due to multiple reflections from several interfaces of this system, no attempt was made to compare the SFG spectra on an absolute signal intensity basis.

Control experiments[34] ensured that the SFG signal originated from the nanoparticles and that the effect of dielectric variations due to density[33] or electronic structure changes within the monolayer was negligible. SFG spectra were collected in *ssp* (SFG-Vis-IR) polarization combination at incident angles greater than the TIR critical angle by 15°. Since other polarization combinations (i.e., *ppp* and *sps*) mainly reflect the dielectric properties of the monolayer,[15] *ssp* polarization was used for the nanoparticle monolayers because of its higher sensitivity to symmetric vibrational modes and higher signal-to-noise ratio. SFG spectra were obtained away from the critical angle for TIR because of the dispersion of the refractive index within the monolayer. At the critical angle, the local electric fields are extremely sensitive to variations in the refractive index.[35]

3. RESULTS AND DISCUSSION

3.1. Nanoparticle Synthesis and Monolayer Formation. Transmission electron microscopy (TEM) revealed that the as-synthesized monolayers consisted of ∼80% cubic and ∼10% tetrahedral nanoparticles (Figure 2A) of average size (largest vertex-to-vertex distance) equal to ∼9 nm and average spacing of a few nm up to 20 nm (calculated for an intermediate surface coverage of 0.4 ML based on the predicted 1−2 nm thickness of the PVP template).[36,37] The predominance of the (111) planes in the nanoparticle structure is evidenced from the X-ray diffractogram shown in Figure 2B. The high-resolution TEM (HR-TEM) image (Figure 2C) and the corresponding Fourier Filtering Transform (FFT) diffraction pattern (Figure 2D) indicate the formation of single-crystal nanoparticles devoid of twinning or any other detectable defects.[27] Reflections from the (200) and (220) planes can also be seen in the FFT diffraction pattern (Figure 2D) of the HR-TEM image shown in Figure 2C.

Previous in situ electron microscopy studies of the same cubic nanoparticles demonstrated nanoparticle edges became rounded upon heating to 623 K in vacuum.[38] This finding is in good agreement with the observed truncation of tetrahedral and cubic Pt nanoparticles capped with sodium polyacrylate in the temperature range of 623−723 K.[39] In view of these findings, low-temperature (373 K) cyclic oxidation−reduction cycles were used to remove the PVP capping agent from the catalyst surface. Nanoparticles were considered "clean" after five oxidation−reduction cycles at 373 K, which is the optimum pretreatment considering both the complete removal of PVP and the maintenance of the particle shape.[40]

3.2. Low- and High-Pressure Adsorption of Ethylene on Pt Single Crystals. Ethylene adsorption on single-crystal Pt(111) and Pt(100) surfaces was first studied at both low (UHV dosing followed by evacuation) and high pressure[41] to establish a reference for ethylene adsorption on the Pt nanoparticle monolayers. A surface species with a resonance at 2903 cm^{-1} was identified upon the exposure of a clean Pt(111) surface to 4L (L = Langmuir, 1 L = 10^{-6} Torr·s) of ethylene at 243 K (Figure 3A). This resonance is attributed to the methylene C−H stretches in di-σ bonded ethylene.[41] Surface annealing at higher temperatures resulted in dehydrogenation of the di-σ bonded ethylene to ethylidyne at ∼280 K, as indicated by the C−H stretch of the ethylidyne methyl group in the range of 2870−2890 cm^{-1}.[41] The ethylidyne species is stable at temperatures above 300 K.[42] An additional resonance at ∼2960 cm^{-1} appeared in the 265 K spectra and disappeared above 281 K. Upon the annealing of adsorbed acetylene on Pt(111) from 125 K to ∼200 K, a resonance at 2960 cm^{-1} attributed to adsorbed ethylidene has been observed previously.[43] The adsorbed ethylidene species was stable up to ∼313 K on a Pt(111) surface that had been saturated with 4L of acetylene. The possible ethylidene species observed on Pt(111) in this study was stable only up to 281 K. The difference in stability of the ethylidene could be related to a stabilization influence of the coadsorbates on the surface which are presumed to be different between acetylene and ethylene at these low adsorption temperatures in the absence of hydrogen.

dx.doi.org/10.1021/cs3005067 | ACS Catal. 2012, 2, 2377−2386

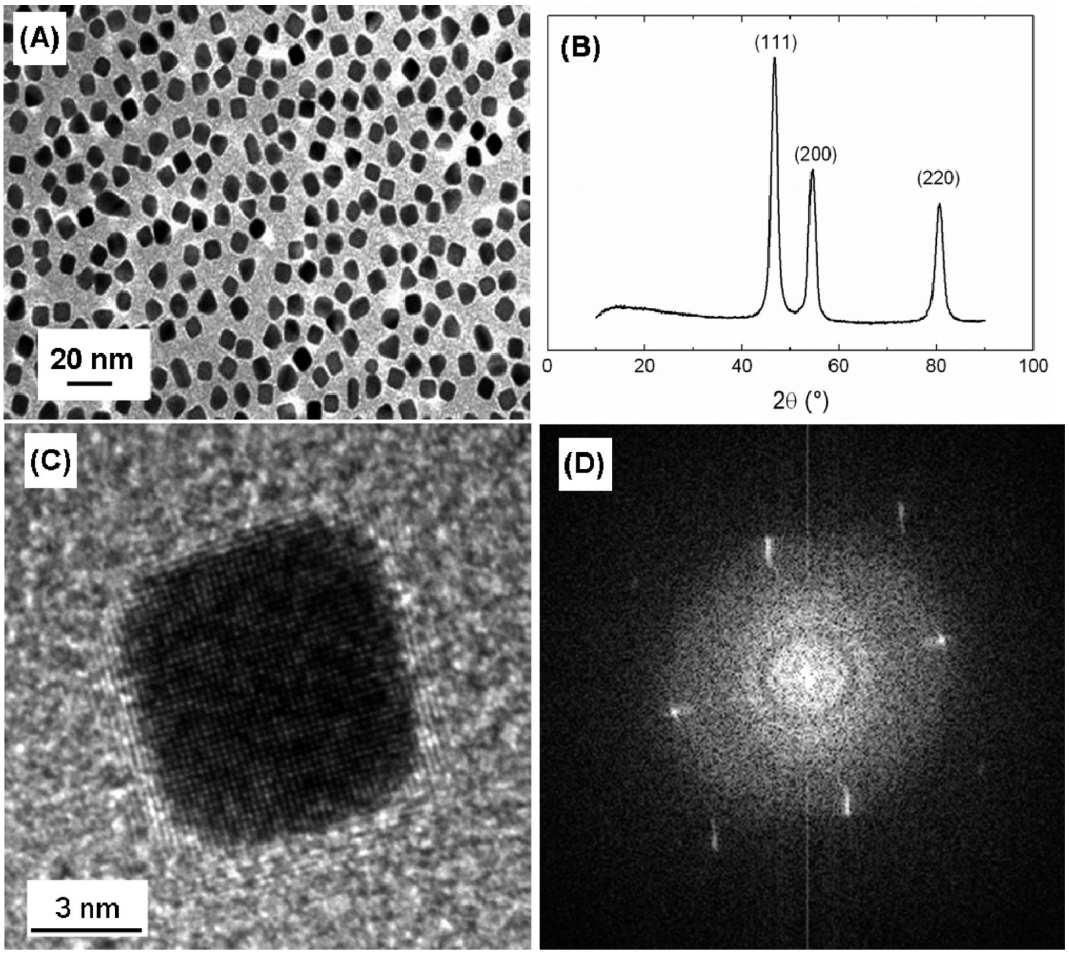

Figure 2. (A) TEM micrograph of PVP-capped Pt nanoparticle monolayer in the as-deposited condition. The Pt nanoparticles were collected onto a carbon-coated Cu grid by the Langmuir–Schäffer technique from a water surface at a surface pressure of 6 mN/m, resulting in a nanoparticle coverage of 0.4 ML.[19,27] (B) X-ray diffractogram of the cubic Pt nanoparticles. The (111)/(200) Bragg reflection ratio reveals a predominantly cubic nanoparticle structure. (C) HR-TEM of a cubic Pt nanoparticle oriented along the [001] zone axis. The distance between adjacent lattice fringes is 1.96 Å, in agreement with the interplanar distance of the (200) plane in the fcc cubic Pt structure.[27] (D) FFT of the image shown in (C). The bright spots are indexed to the (200) and (220) planes.

A single C–H resonance at 2900 cm^{-1} was observed in the spectrum of low-pressure adsorption of ethylene on a clean Pt(100) single crystal at 140 K (Figure 3B). The position of this peak (assigned to di-σ bonded ethylene) was not affected by subsequent heating. Unlike Pt(111), di-σ bonded ethylene did not dehydrogenate to ethylidyne on the Pt(100) surface. The intensity of the di-σ bonded ethylene decreased with an increase in temperature until it completely disappeared without any evidence for ethylidyne formation. At 140 K, di-σ bonded ethylene adsorbs at 3-fold hollow sites on the (5 × 20) Pt(100) surface. The Pt(100) crystal face reconstructs to a pseudohexagonal structure, known as (5 × 20) Pt(100)[44] or Pt(100)-*hex*,[45] resembling the hexagonal structure of Pt(111) when properly cleaned in vacuum.[45,46] The second layer retains the square array of the (100) surface. The reconstruction of the ideal (1 × 1) surface to the pseudohexagonal (5 × 20) surface decreases the total surface energy by 17%.[47] At a higher temperature (~260 K), the (5 × 20) structure reconstructs to the metastable (1 × 1) structure before the di-σ bonded ethylene can be converted to ethylidyne. After surface reconstruction, ethylidyne does not form on the (1 × 1) surface because it lacks 3-fold hollow sites. On the Pt(111) crystal surface, the di-σ species converted to ethylidyne at 273 K (Figure 3A).

At high pressures of ethylene (>5 × 10^{-7} Torr), both di-σ bonded ethylene and ethylidyne formed on Pt(100), as shown in Figure 4A. On the Pt(100) surface, the ethylidyne stretching frequency was observed at ~2880 cm^{-1} and the di-σ bonded ethylene stretching frequency at 2910 cm^{-1}. Both ethylidyne and di-σ bonded ethylene adsorb at fcc 3-fold hollow sites, with the molecular axis of the di-σ bonded ethylene tilted with respect to the surface plane by ~22°.[42] Upon exposure to 1 × 10^{-7} Torr of ethylene, the (5 × 20) Pt(100) surface (monitored by LEED) reconstructed back to the (1 × 1) structure. Previous LEED measurements demonstrated a diffuse (1 × 1) pattern, indicating that the pseudohexagonal reconstruction is lifted with a high degree of disorder for an ethylene coverage of ~0.5 ML.[48] This disorder may result in the formation of ensembles that retain the ⟨111⟩ orientation, allowing ethylidyne to remain stable even after surface reconstruction.

3.3. High-Pressure Ethylene Adsorption on Clean Pt Nanoparticle Monolayers. The surface chemistry of ethylene on both planar and nanoparticle transition metal surfaces has been studied extensively.[41] Most previous studies have been focused on the adsorption, decomposition, and hydrogenation

dx.doi.org/10.1021/cs3005067 | *ACS Catal.* 2012, 2, 2377–2386

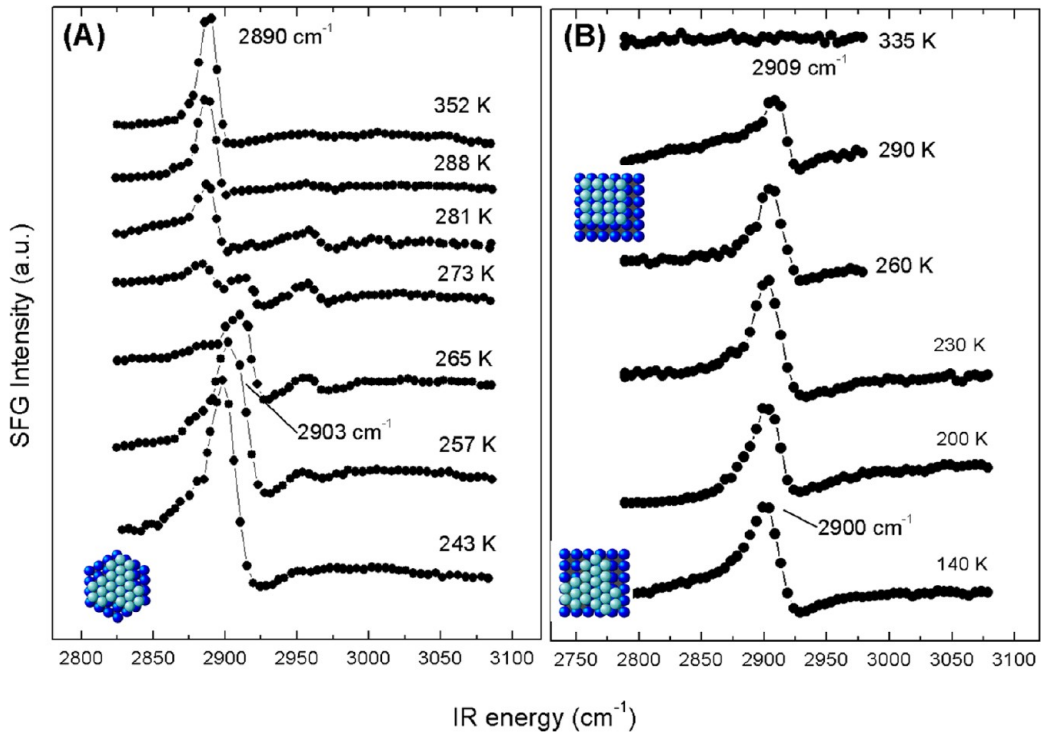

Figure 3. (A) Low-pressure exposure of Pt(111) single crystal to ethylene at 243 K and annealing up to 352 K. Heating causes the di-σ bonded ethylene (~2900 cm^{-1}) formed upon ethylene adsorption to dehydrogenate to ethylidyne (~2890 cm^{-1}). The conversion from adsorbed ethylene to ethylidyne occurs at ~273 K. (B) Low-pressure exposure of a single-crystal Pt(100) surface with a pseudohexagonal reconstructed surface to ethylene at 140 K and annealing up to 335 K. Ethylene adsorbs initially at 140 K as di-σ bonded ethylene at 3-fold hollow sites. The increase of the temperature leads to decomposition (or desorption) of the di-σ bonded ethylene and the reconstruction of the pseudohexagonal (5 × 20) Pt(100) surface to the (1 × 1) Pt(100).[47,48] The inset in (A) shows a model of the Pt(111) surface, whereas the lower and upper insets in (B) show models of the pseudohexagonal (5 × 20) Pt(100) and (1 × 1) Pt(100) surfaces, respectively. The light blue atoms represent the outermost (surface) layer, while the blue atoms are those that make up the second layer.

of ethylene on Pt(111). The C−H stretching frequency of ethylene species (i.e., π-bonded and di-σ bonded ethylene) molecularly adsorbed on Pt(111) are at ~2990 and ~2910 cm^{-1}, respectively. Dehydrogenated species, such as ethylidyne (Pt_3C-CH_3)[49] and ethylidene ($Pt_2CH{=}CH_2$),[50] have also been observed on the Pt(111) facet with most prominent C−H stretching frequencies of ~2875 and ~2960 cm^{-1}, respectively. Ethylidene is hydrogenated to ethylene at very mild conditions and is generally observed under UHV conditions,[50] whereas ethylidyne is stable from UHV conditions up to atmospheric hydrogen conditions.[51]

The SFG spectrum of high-pressure ethylene adsorption on the Pt nanoparticle monolayer after cyclic oxidation−reduction treatment (Figure 4C) is compared with those of Pt(100) (Figures 4A and 4B) and Pt(111) (inset of Figure 4C). The two peaks at 2875 and 2910 cm^{-1} are associated with the methyl stretch of ethylidyne and the methylene stretch of di-σ bonded ethylene, respectively. Both species are stable on Pt(100) up to 300 K under high-pressure adsorption (Figure 4A) and hydrogenation (Figure 4B) conditions.[52] The di-σ species previously identified on Pt(100)[44,53,54] are also expected to form on the cubic Pt nanoparticles.

A main difference between nanoparticle and planar surfaces is the presence of edge and corner atoms on the cubic nanoparticles, although the estimated fraction of edge and corner atoms at the surface of a 9 nm, perfectly cubic Pt particle is less than 1%.[55] Even though the fraction of these sites is small, their reduced coordination number may result in increased reactivity and spectroscopic signatures of more highly dehydrogenated species.[54,56] The di-σ species is stable on the Pt nanoparticle monolayer up to at least 300 K, consistent with the behavior observed with Pt single crystals.

The second species observed on the nanoparticle monolayer is believed to be ethylidyne (Pt_3C-CH_3). Ethylidyne formation on Pt(111) (inset of Figure 4C) has been observed in earlier SFG studies.[5,49,57] The similarity of the shape and band positions of the Pt(111) spectrum with those of the spectrum shown in Figure 4C suggest that the species observed on the nanoparticle monolayer is ethylidyne. According to an ethylidyne model derived from LEED studies,[42] the preferred binding of ethylidyne is in 3-fold coordinated sites. Since defect-free Pt cubic nanoparticles exhibit 4-fold symmetry, ethylidyne should not form on cubic nanoparticles because of the lack of 3-fold coordination sites.

The conversion of molecularly adsorbed ethylene does not have to proceed through the formation of an ethylidyne intermediate. In fact, several studies[44,51−54,58−60] have demonstrated that ethylidyne does not form on a number of Pt surfaces. The surface most related to the current work is Pt(100). In vacuum, the metastable (1 × 1) Pt(100) surface reconstructs to a pseudohexagonal (5 × 20) Pt(100) surface[56,61] and is stable to ethylene adsorption.[44,52] Surface intermediates formed upon the decomposition of low-pressure ethylene are different on these surfaces. Specifically, ethylidyne formed on the pseudohexagonally reconstructed surface, whereas high-resolution electron energy loss spectroscopy (HREELS) and temperature-controlled desorption studies have provided evidence for the formation of vinylidene

dx.doi.org/10.1021/cs3005067 | ACS Catal. 2012, 2, 2377−2386

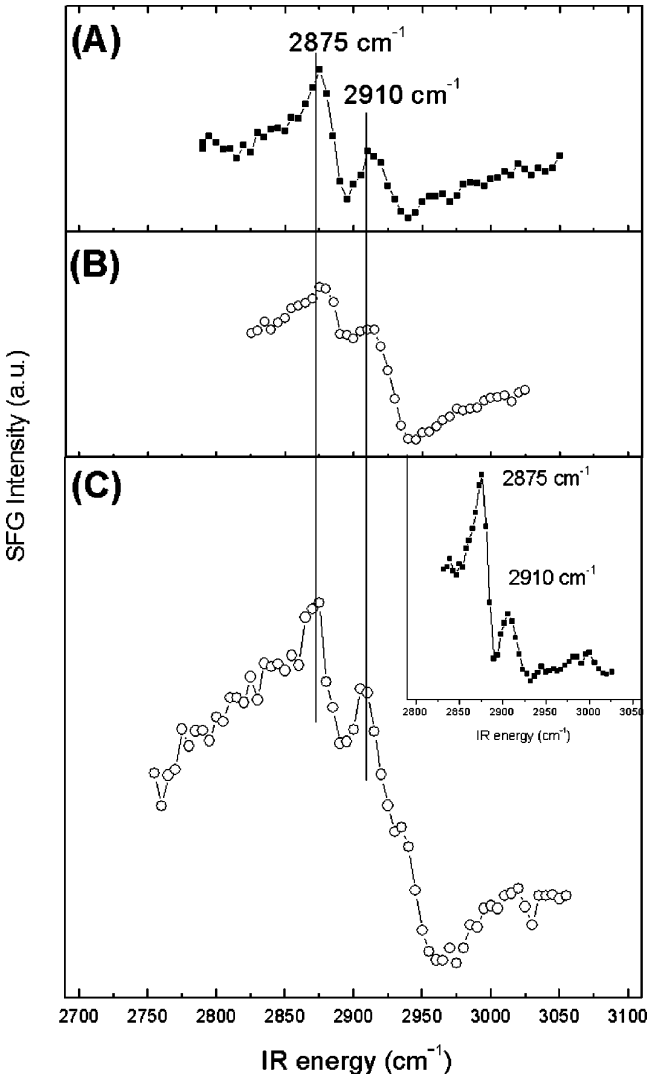

Figure 4. SFG spectra of high-pressure ethylene adsorption on Pt single crystals and PVP-capped Pt nanoparticle monolayer at room temperature. Adsorption of ethylene at (A) 5×10^{-7} Torr C_2H_4 on Pt(100); (B) 35 Torr C_2H_4 and 100 Torr H_2 on Pt(100); and (C) 700 Torr C_2H_4 on a clean Pt nanoparticle monolayer. The inset in (C) shows the SFG spectrum of a Pt(111) surface exposed to high-pressure ethylene hydrogenation conditions (35 Torr C_2H_4 and 100 Torr H_2).[31] Regardless of the exposed surface structure and/or presence of hydrogen, the positions of the ethylidyne and di-σ bonded ethylene peaks are identical under high-pressure adsorption conditions.

($Pt_2CH{=}CH_2$) and acetylenic ($Pt_2CH{-}CHPt_2$, quad-σ acetylene) intermediates on the (1 × 1) Pt(100) surface.[52] The dehydrogenated C_2 intermediates on the (1 × 1) surface produce C−H resonances in the HREELS spectrum at 2968 and 2984 cm^{-1}, respectively, which are significantly blue-shifted from the resonances observed in the spectrum of the cubic Pt nanoparticles (Figure 4C). Therefore, vinylidenic and acetylenic species are not considered to be potential stable surface intermediates on the cubic nanoparticles.

CO adsorption results for surface coverage greater than 0.5 ML have shown that the pseudohexagonal (5 × 20) Pt(100) surface reconstructs to the (1 × 1) Pt(100) surface.[62] It is possible that this coverage of ethylene does not completely lift the reconstruction as in the case of high surface coverage by CO. This is supported by LEED results showing that the (5 × 20) surface at saturation coverage reconstructs to the metastable (1 × 1) surface containing a high density of defects. Although the (5 × 20) Pt(100) surface is stable at low ethylene pressures,[44,52] the stability of the pseudohexagonal surface in the presence of high-pressure ethylene is not known. The preferred adsorption for ethylidyne is in 3-fold hollow sites, a geometrical ensemble present on pseudohexagonal surfaces, which may stabilize a portion of the (5 × 20) surface.

The cubic nanoparticles may also be terminated by facets other than (100). HR-TEM images revealed cubic nanoparticles with rounded corners, while electron diffraction showed that the Pt cubes possessed a lattice fringe spacing of 1.96 Å, in agreement with the interplanar distance of the (200) plane, indicating a defect-free bulk.[27] It is not known if the nanoparticle surfaces are terminated by (100) facets only or if defects also exist. A HR-TEM study of cubic Pt nanoparticles synthesized from sodium polyacrylate demonstrated that cubic particles commonly have rounded corners, where steps and kinks may congregate.[63] Irregularly shaped cubic particles are terminated not only by (100) surfaces but also by (111) and (110) surfaces. The adsorption of ethylene on small metal crystallites has been studied in depth.[41,64,65] It has been proposed that the formation of ethylidyne on metal crystallites is an indicator of the fraction of particle surfaces terminated by (111) facets.[66] Vibrational coupling of adsorbed $^{13}C_2H_4/^{12}C_2H_4$ shows that ethylidyne is produced on (111) facets of Pt particles (d = 10−40 Å, average = 20 Å) rather than on random trimer Pt sites.[67] This suggests that although the surface may become defective upon its transition from the (5 × 20) to the (1 × 1) surface, hexagonally oriented facets rather than random trimer sites are stabilized by high-pressure ethylene adsorption.

3.4. Characterization of Capping Polymer and Restructuring Due to CO Adsorption. Surface stabilizing agents used in solution-phase nanoparticle synthesis prevent particle aggregation[24,27,68−72] and may also contribute to size and shape control.[73] The interaction between PVP and metal ions occurs through the C═O group of the pyrrolidone ring, and the ability of monomer units of the polymer chain to interact (intramolecular) with other sections containing Pt ions promotes the aggregation of metal ions and, subsequently, the formation of nanoparticles.[74]

The coordination of PVP to cubic Pt nanoparticles was studied by SFG vibrational spectroscopy. A PVP monolayer spun cast from a 5 wt.% chloroform solution onto a clean α−Al_2O_3(0001) prism was used as a control. The SFG spectrum with *ssp* polarization of the sapphire/PVP interface in the C−H stretching region, shown in Figure 5A, contains two broad peaks at 2895 and 2995 cm^{-1}, assigned to the symmetric stretch of the methylene groups in the pyrrolidone ring (CH_2(s)) and asymmetric methylene stretches (CH_2(as)) of the vinyl backbone of PVP. The shoulders observed at ∼2865 and ∼2930 cm^{-1} are assigned to a tertiary C−H stretch and the CH_2(s) stretch of the vinyl chain, respectively. These peak positions are in good agreement with reported values from IR and Raman spectroscopy.[75,76] However, because of the complicated nature of the interface, no attempt was made to deconvolute the spectrum to determine contributions from multiple C−H resonances and individual peak intensities. The CH_2(s) peak intensity of the pyrrolidone ring indicates that the polymer is ordered with the pyrrolidone ring and vinyl backbone lying flat against the sapphire surface. Polymers at

dx.doi.org/10.1021/cs3005067 | ACS Catal. 2012, 2, 2377−2386

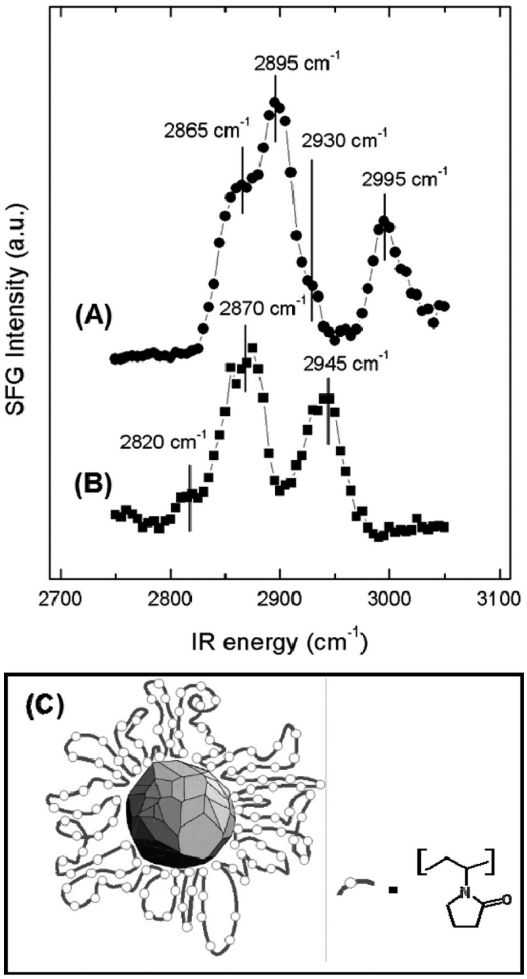

Figure 5. SFG spectra of sapphire/PVP and sapphire/Pt nanoparticle monolayer obtained with *ssp* polarization. (A) C−H stretching region of the sapphire/PVP interface. The PVP monolayer was spun-cast from a 5 wt % chloroform solution. The symmetric CH_2 stretch [CH_2(s)] of the pyrrolidone ring and the asymmetric CH_2 stretch [CH_2(as)] of the vinyl backbone are at 2895 and 2995 cm^{-1}, respectively. The shoulders are assigned to a tertiary C−H stretch (~2865 cm^{-1}) and a CH_2(s) stretch (~2930 cm^{-1}) of the vinyl backbone. The intensity of the CH_2(s) peak of the pyrrolidone ring indicates that the polymer chains are well-ordered and the ring and backbone lay against the sapphire surface. (B) C−H stretching region of the PVP/Pt nanoparticle monolayer system. All resonances in this wavelength region are attributed to PVP bound to the nanoparticle surface. The CH_2(s) stretch (2870 cm^{-1}) of the pyrrolidone ring and the CH_2(as) stretch (2945 cm^{-1}) of the vinyl backbone are red-shifted by 25−50 cm^{-1} relative to corresponding peaks in the spectrum of the PVP spun-cast film. (C) Model of PVP bound to a Pt nanoparticle of an arbitrary shape.[83] It is envisioned in solution PVP contacts the Pt surface through a small fraction of the C═O groups along the length of a single polymer chain.

solid surfaces behave differently than in the bulk; specifically, polymer chains in the bulk bunch randomly. If the domains of bunched chains are truly random, they will not produce a SFG signal. The high intensities of the CH_2(s) resonances in Figure 5A are associated with a surface layer consisting of ordered chains.

The SFG spectrum of the PVP-capped Pt nanoparticle monolayer, shown in Figure 5B, contains two dominant peaks at 2870 and 2945 cm^{-1}, attributed to CH_2(s) vibrations of the pyrrolidone ring and vinyl backbone, respectively. These peaks are red-shifted by 25−50 cm^{-1} relative to corresponding peaks in the spin-cast PVP/sapphire spectrum (Figure 5A). This suggests an electron density donation from PVP to Pt.[75] It has been proposed that PVP strongly adsorbs to the surfaces of metal nanoparticles via the carbonyl bond.[77−79] The C═O frequency red-shifts by as much as 60 and 45 cm^{-1} for 8 and 3 nm Pt nanoparticles, respectively,[75] relative to the IR liquid-phase frequency.[80] In another study, a significantly smaller red-shift of 15 cm^{-1} was obtained with 2.5 nm Pt nanoparticles.[81] A red-shift of the C═O frequency by 20 cm^{-1} was observed in the case of 70-nm-diameter Ag nanowires.[79] Detecting the red-shift of the C═O frequency was not possible in the present study because of the limited power of the SFG setup at C═O stretching energies (~1670 cm^{-1}). Surface-enhanced Raman spectroscopy studies of PVP coordination to Ag nanowires suggest that the pyrrolidone ring is tilted relative to the surface and the vinyl backbone is close to the Ag surface.[78] The SFG spectra of PVP-Pt coordination is in qualitative agreement with the proposed PVP-Ag coordination. The change in the line-shape of the methylene peaks from the spectrum of the spin-cast PVP film (Figure 5A) to the spectrum of the PVP/Pt nanoparticle monolayer interface (Figure 5B) is probably due to variations in the average orientation of the polymer chains caused by substrate morphology. A similar argument was used to interpret differences between the SFG spectra of dioctadecyldimethylammonium chloride monolayers adsorbed on single-crystal Si and Au nanoparticle layers.[82]

Figure 5C shows a model of a PVP-capped Pt nanoparticle with an arbitrary shape in solution.[83] The PVP polymer contacts the Pt surface through a small fraction of the C═O groups along the length of a single polymer chain. It is believed that the PVP layer in solution is quite flexible, whereas in the dry state (i.e., LB monolayer) it collapses to form a dense polymer coating around the nanoparticles. Dendrimer-stabilized Pt nanoparticles can adsorb CO in solution but not in the dry state, presumably because of the collapse of the dendrimer around the nanoparticles.[84]

The adsorption of CO on PVP-capped Pt nanoparticles suggests that the PVP layer is extremely flexible even after drying. This enhances CO adsorption, which, in turn, causes PVP to restructure from an ordered to a disordered state (Figures 6A and 6B). This transition is a qualitative observation based entirely on the decrease of the SFG intensities of backbone methylene resonances. The intensities of both CH_2(s) and CH_2(as) stretches of the vinyl backbone decrease upon CO adsorption. The CO stretching frequency (2065 cm^{-1}) is red-shifted by 10 cm^{-1} relative to that corresponding to CO adsorption on a Pt nanoparticle monolayer calcined in O_2 at 373 K for 3 h (2075 cm^{-1})[19] (inset of Figure 6). These observations support a possible transfer of charge from PVP to CO mediated through the metal surface.[75] The exposure of the Pt monolayer to oxygen leads to the removal of CO by oxidation and the restructuring of the PVP adlayer.

The conformational change of PVP upon CO adsorption-removal by mild oxidation appears to be partially reversible, although the initial intensity of the CH_2(as) stretch is not fully recovered (Figure 6C). The ability of CO to adsorb is most likely due to a porous PVP layer; thus, the nanoparticles may be catalytically active before the removal of the polymer.[85,86] In solution, interaction of the polymer with the nanoparticle surface is dynamic, causing polymer conformation to change and allowing small adsorbates to access the surface. H_2−O_2 titration and H_2 chemisorption on PVP-protected Pt colloids in

dx.doi.org/10.1021/cs3005067 | ACS Catal. 2012, 2, 2377−2386

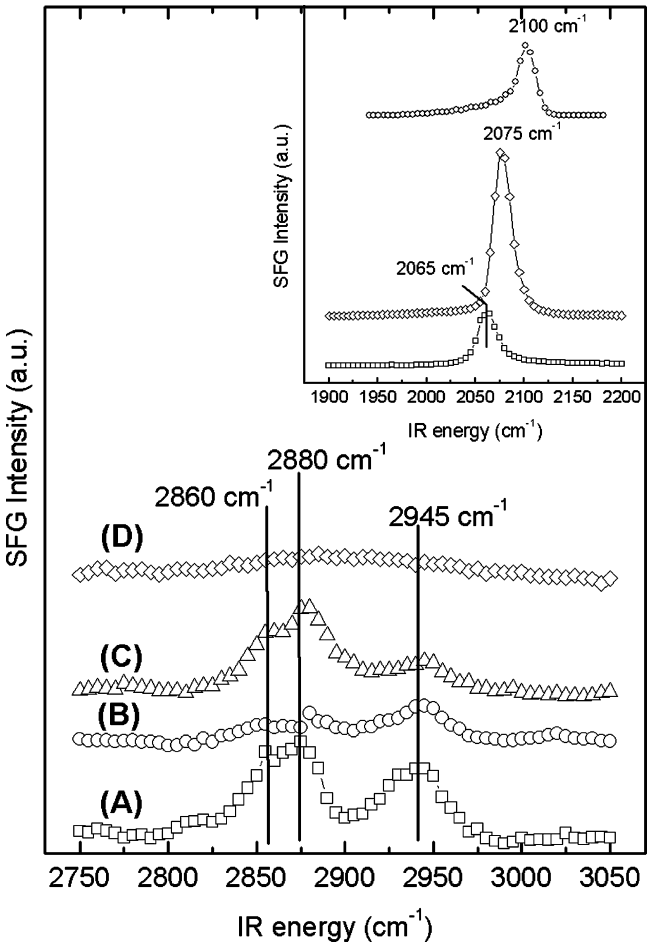

Figure 6. Effect of CO adsorption on restructuring of the PVP layer. SFG spectrum of PVP-capped Pt nanoparticle monolayer: (A) as-synthesized condition, (B) after exposure to 700 Torr of CO, (C) after CO removal by exposure to air (room temperature CO oxidation), and (D) after five cycles of oxidation−reduction treatment at 373 K. The inset shows the CO stretching frequency regime of the PVP-capped Pt nanoparticle monolayer in (□) the as-synthesized condition and (◇) after five oxidation−reduction cycles at 373 K and (○) the (1 × 1) Pt(100) surface.[30]

solution demonstrated that ∼50% of the nanoparticle surface area was available for CO adsorption.[87] Vibrational (dipole) coupling between adsorbed CO molecules suggested that the free Pt surface is in the form of small ensembles. The dried surface of the Pt nanoparticles was exposed to CO pressure on the order of ∼1 Torr, and all surface sites available for CO adsorption were saturated. In this work, a band position at 2065 cm^{-1} most likely reflects the interaction of CO with coadsorbed polymer and not dipole coupling, as was observed in a previous infrared spectroscopy study.[75] In the case of dried nanoparticles, it is presumed that Pt atoms free of PVP are isolated in ensembles, producing a very small fraction of nanoparticle surface available for adsorption (and reaction). Catalytic reactivity results have shown that PVP-coated Pt nanoparticles on mesoporous SBA-15 silica are active for ethylene hydrogenation, although their activity is smaller by a factor of 30−50 than that of catalysts subjected to calcination and reduction pretreatment.[40]

3.5. PVP Removal from the Nanoparticle Surface by Cyclic Oxidation−Reduction. The removal of surface protecting agents (such as PVP) from the nanoparticle surfaces is an important step for maximizing nanoparticle efficiency in gas-phase heterogeneous catalysis.[85,86] The removal of PVP from the dried nanoparticle surface is challenging because of its strong coordination to the Pt nanoparticle surface, high molecular weight, and collapse and densification by cross-linking of the PVP monolayer after drying.[75] A cyclic oxidation−reduction procedure at low temperatures (373 K) has been developed to remove the PVP layer from the surfaces of Pt nanoparticles supported on mesoporous silica. This method was applied to the Pt nanoparticle LB layers fabricated in this study. The use of ozone has proven to be an effective method for the removal of PVP from the surface of Pt[88] or Pd[89] nanoparticles without disturbing the particle size or shape, respectively. Additional solvent rinsing of PVP-covered Pt nanoparticles at the stage of synthetic workup and purification has been used effectively to remove excess PVP from the surface of the nanoparticles, but surface bound PVP was still identified by SFG spectroscopy.[90] Figure 6A shows peaks assigned to PVP that are clearly identified on the nanoparticle surface after synthesis and monolayer assembly. The intense bands in the C−H stretching region suggest that PVP is well ordered at the surface, whereas the significant shift to lower energy suggests that PVP is strongly coordinated to the surface. After five oxidation−reduction cycles at 373 K, the SFG spectrum (Figure 6D) of the sapphire/nanoparticle interface in oxygen at room temperature is essentially featureless, suggesting that either PVP was completely removed or the small fraction of PVP that remained at the surface after oxidation−reduction treatment is disordered. The rate of olefin hydrogenation on supported Pt catalysts increased after each oxidation−reduction cycle, reaching a steady-state after five cycles at 373 K.[40] In view of these results, the lack of SFG signals in Figure 6D is attributed to the removal of PVP rather than the presence of a disordered PVP adlayer.

Changes in the SFG spectra following cyclic oxidation−reduction become evident when comparing the adsorption of CO before and after cyclic oxidation−reduction pretreatment (inset of Figure 6). Prior to the oxidation−reduction treatment, the SFG spectrum shows a single peak at 2065 cm^{-1}, which is red-shifted by ∼35 cm^{-1} relative to the peak (2100 cm^{-1}) corresponding to CO adsorption on single-crystal (1 × 1) Pt(100).[30] The intensity of the atop CO peak increased by a factor of 2, and its position blue-shifted by 10 cm^{-1} to 2075 cm^{-1} after five oxidation−reduction cycles at 373 K because of the combustion of the PVP layer.[19]

4. CONCLUSIONS

SFG vibrational spectroscopy in TIR geometry was used to characterize the adsorption of ethylene on a monolayer film consisting of 9-nm average size, cubic Pt nanoparticles after removal of the PVP polymer by an oxidation−reduction treatment. Comparison of results for high-pressure adsorption of ethylene on clean nanoparticle monolayers with results from UHV and high-pressure adsorption of ethylene on Pt(100) single crystals indicated that high-pressure ethylene partially stabilized the pseudohexagonal (5 × 20) Pt(100) surface on both the Pt(100) surface and the cubic Pt nanoparticles. The interaction of the surface template polymer (PVP) with the surface of cubic Pt nanoparticles and its removal by cyclic oxidation−reduction were investigated by TIR-SFG. The presence of PVP on the surface of the Pt nanoparticles decreased the adsorption capacity, and caused a red-shift of the linear-bound CO peak relative to CO adsorption on a

dx.doi.org/10.1021/cs3005067 | ACS Catal. 2012, 2, 2377−2386

nanoparticle monolayer subjected to oxidation−reduction cycles. CO adsorption on PVP-capped Pt nanoparticles led to significant restructuring of the PVP layer, which was partially reversible upon the removal of CO by low-temperature oxidation. The amount of adsorbed CO increased and the peak position of the linear-bound CO peak blue-shifted relative to CO adsorption on the PVP-capped Pt nanoparticle monolayer with a simultaneous attenuation of the resonances, attributed to the removal of the PVP layer after low-temperature (373 K) cyclic oxidation−reduction treatment. The application of an inherently surface-specific spectroscopy technique, such as SFG vibrational spectroscopy, to the study of rough surfaces (e.g., nanoparticles) demonstrated in this investigation is a major advance in the in situ characterization of heterogeneous catalysts.

AUTHOR INFORMATION

Corresponding Author

*E-mail: somorjai@berkeley.edu (G.A.S.), rioux@engr.psu.edu (R.M.R.).

Present Addresses

[‖]MEMC Electronic Materials, 501 Pearl Drive, St. Peters, MO 63376-0008.

[⊥]Department of Chemical Engineering, The Pennsylvania State University, University Park, PA 16802.

[⊗]Department of Chemistry and School of Molecular Science (BK21), Korea Advanced Institute of Science and Technology, Daejeon, 305-701, Korea.

Funding

This work was supported by the Director, Office of Science, Office of Advanced Scientific Computing Research, Office of Basic Energy Sciences, Materials Sciences and Engineering Division, of the U.S. Department of Energy under Contract No. DE-AC02-05CH11231. R.M.R. would like to acknowledge Ford Motor Company for financial support through a graduate fellowship administered by the Berkeley Catalysis Center.

Notes

The authors declare no competing financial interest.

REFERENCES

(1) Rupprechter, G. *Annu. Rep. Prog. Chem., Sect. C: Phys. Chem.* **2004**, *100*, 237.

(2) Freund, H. J.; Libuda, J.; Baumer, M.; Risse, T.; Carlsson, A. *Chem. Rec.* **2003**, *3*, 181.

(3) Rupprechter, G.; Weilach, C. *Nano Today* **2007**, *2*, 20.

(4) Somorjai, G. A.; York, R. L.; Butcher, D.; Park, J. Y. *Phys. Chem. Chem. Phys.* **2007**, *9*, 3500.

(5) Cremer, P. S.; Su, X. C.; Somorjai, G. A.; Shen., Y. R. *J. Mol. Catal. A: Chem.* **1998**, *131*, 225.

(6) Dellwig, T.; Hartmann, J.; Libuda, J.; Meusel, I.; Rupprechter, G.; Unterhalt, H.; Freund, H. J. *J. Mol. Catal. A: Chem.* **2000**, *162*, 51.

(7) Foster, A. J.; Lobo, R. F. *Chem. Soc. Rev.* **2010**, *39*, 4783.

(8) Buck, M.; Himmelhaus, M. *J. Vac. Sci. Technol., A* **2001**, *19*, 2717.

(9) Raschke, M. B.; Shen, Y. R. *Curr. Opin. Solid State Mater. Sci.* **2004**, *8*, 343.

(10) Somorjai, G. A. *Appl. Surf. Sci.* **1997**, *121*, 1.

(11) Somorjai, G. A.; Rupprechter, G. *J. Phys. Chem. B* **1999**, *10*, 1623.

(12) Vidal, F.; Tadjeddine, A. *Rep. Prog. Phys.* **2005**, *68*, 1095.

(13) Shen, Y. R. *Pure Appl. Chem.* **2001**, *73*, 1589.

(14) Somorjai, G. A.; McCrea, K. R. *Adv. Catal.* **2000**, *45*, 385.

(15) Baldelli, S.; Eppler, A. S.; Anderson, E.; Shen, Y. R.; Somorjai, G. A. *J. Chem. Phys.* **2000**, *113*, 5432.

(16) Rupprechter, G.; Freund, H. J. *Top. Catal.* **2001**, *14*, 3.

(17) Unterhalt, H.; Rupprechter, G.; Freund, H. J. *J. Phys. Chem. B* **2002**, *106*, 356.

(18) Ma, G.; Allen, H. C. *J. Am. Chem. Soc.* **2002**, *124*, 9374.

(19) Kweskin, S. J.; Rioux, R. M.; Habas, S. E.; Komvopoulos, K.; Yang, P.; Somorjai, G. A. *J. Phys. Chem. B* **2006**, *110*, 15920.

(20) Yeganeh, M. S.; Dougal, S. M.; Sibernagel, B. G. *Langmuir* **2006**, *22*, 637.

(21) Waldrup, S. B.; Williams, C. T. *Catal. Commun.* **2007**, *8*, 1373.

(22) Bratlie, K. M.; Komvopoulos, K.; Somorjai, G. A. *J. Phys. Chem. C* **2008**, *112*, 11865.

(23) Kliewer, C. J.; Aliaga, C.; Bieri, M.; Huang, W. Y.; Tsung, C. K.; Wood, J. B.; Komvopoulos, K.; Somorjai, G. A. *J. Am. Chem. Soc.* **2010**, *132*, 13088.

(24) Ott, L. S.; Hornstein, B. J.; Finke, R. G. *Langmuir* **2006**, *22*, 9357.

(25) Teranishi, T.; Hosoe, M.; Tanaka, T.; Miyake, M. *J. Phys. Chem. B* **1999**, *103*, 3818.

(26) Wang, Y.; Ren, J.; Deng, K.; Gui, L.; Tang, Y. *Chem. Mater.* **2000**, *12*, 1622.

(27) Song, H.; Kim, F.; Connor, S.; Somorjai, G. A.; Yang, P. D. *J. Phys. Chem. B* **2005**, *109*, 188.

(28) Langmuir, I.; Schaefer, V. J.; Wrinch, D. M. *Science* **1937**, *85*, 76.

(29) The spectra of adsorbed intermediates were collected under UHV and high-pressure conditions. For low-pressure experiments, ethylene was dosed into the chamber through a leak valve at low pressures (10^{-8}−10^{-7} Torr) for a specified amount of time. The low-pressure exposure is stated in units of Langmuir. After exposure, the supply of gas was eliminated, and the chamber was pumped down to a vacuum of $< 10^{-9}$ Torr before spectra were collected or the single crystal was heated. For high pressure experiments, the chamber was supplied with a constant pressure of ethylene—equilibrium between gas-phase and adsorbed ethylene—during spectra collection and sample heating.

(30) McCrea, K.; Parker, J. S.; Chen, P.; Somorjai, G. *Surf. Sci.* **2001**, *494*, 238.

(31) McCrea, K. R.; Somorjai, G. A. *J. Mol. Catal. A: Chem.* **2000**, *163*, 43.

(32) Pang, S. F.; Kurosawa, Y.; Kondo, T.; Kawai, T. *Chem. Lett.* **2005**, *34*, 544.

(33) This refers to the strong dependence of the magnitude of the imaginary component of the dielectric constant of Pt on the wavelength of the incident light.

(34) Control experiments included the collection of the SFG spectrum of the sapphire surface, as well as the SFG spectrum of the sapphire surface after CO adsorption without a monolayer of nanoparticles (i.e., bare sapphire in air).

(35) York, R. L.; Li, Y. M.; Holinga, G. J.; Somorjai, G. A. *J. Phys. Chem. A* **2009**, *113*, 2768.

(36) Reetz, M. T.; Helbig, W.; Quaiser, S. A.; Stimming, U.; Breuer, N.; Vogel, R. *Science* **1995**, *267*, 367.

(37) Su, M.; Bai, C. L.; Wang, C. *Solid State Commun.* **1998**, *106*, 643.

(38) Yu, R.; Song, H.; Zhang, X. F.; Yang, P. *J. Phys. Chem. B* **2005**, *109*, 6940.

(39) Wang, Z. L.; Petroski, J. M.; Green, T. C.; El-Sayed, M. A. *J. Phys. Chem. B* **1998**, *102*, 6145.

(40) Rioux, R. M.; Song, H.; Grass, M.; Habas, S.; Niesz, K.; Hoefelmeyer, J. D.; Yang, P.; Somorjai, G. A. *Top. Catal.* **2006**, *39*, 167.

(41) Sheppard, N.; Cruz, C. D. L. *Adv. Catal.* **1996**, *41*, 1.

(42) Starke, U.; Barbieri, A.; Materer, N.; Hove, M. A. V.; Somorjai, G. A. *Surf. Sci.* **1993**, *286*, 1.

(43) Cremer, P. S.; Su, X. C.; Shen, Y. R.; Somorjai, G. A. *J. Phys. Chem. B* **1997**, *101*, 6474.

(44) Hatzikos, G. H.; Masel, R. I. *J. Vac. Sci. Technol., A* **1987**, *5*, 831.

(45) Heilmann, P.; Heinz, K.; Müller, K. *Surf. Sci.* **1979**, *83*, 487.

(46) Broden, G.; Pirug, G.; Bonzel, H. P. *Surf. Sci.* **1978**, *72*, 45.

(47) Yeo, Y. Y.; Wartnaby, C. E.; King, D. A. *Science* **1995**, *268*, 1731.

(48) Yeo, Y. Y.; Stuck, A.; Wartnaby, C. E.; Kose, R.; King, D. A. *J. Mol. Catal. A: Chem.* **1998**, *131*, 31.

(49) Cremer, P.; Stanners, C.; Niemantsverdriet, J. W.; Shen, Y. R.; Somorjai, G. A. *Surf. Sci.* **1995**, *328*, 111.
(50) Deng, R. P.; Herceq, E.; Trenary, M. *Surf. Sci.* **2004**, *560*, L195.
(51) Backman, A. L.; Masel, R. I. *J. Vac. Sci. Technol., A* **1991**, *9*, 1789.
(52) Hatzikos, G. H.; Masel, R. I. *Surf. Sci.* **1987**, *185*, 479.
(53) Yagasaki, E.; Backman, A. L.; Masel, R. I. *Vacuum* **1990**, *41*, 57.
(54) Yagasaki, E.; Backman, A. L.; Masel, R. I. *J. Vac. Sci. Technol., A* **1990**, *8*, 2610.
(55) Hardeveld, R. V.; Hartog, F. *Surf. Sci.* **1969**, *15*, 189.
(56) Lyon, H. B.; Somorjai, G. A. *J. Chem. Phys.* **1967**, *46*, 2539.
(57) Cremer, P. S.; Su, X. C.; Shen, Y. R.; Somorjai, G. A. *J. Am. Chem. Soc.* **1996**, *118*, 2942.
(58) Backman, A. L.; Masel, R. I. *J. Vac. Sci. Technol., A* **1988**, *6*, 1137.
(59) Backman, A. L.; Masel, R. I. *J. Phys. Chem.* **1990**, *94*, 5300.
(60) Yagasaki, E.; Backman, A. L.; Masel, R. I. *J. Phys. Chem.* **1990**, *94*, 1066.
(61) Somorjai, G. A. *Catal. Rev.* **1972**, *7*, 87.
(62) Behm, R. J.; Thiel, P. A.; Norton, P. R.; Ertl, G. *J. Chem. Phys.* **1983**, *78*, 7437.
(63) Wang, Z. L.; Ahmad, T. S.; El-Sayed, M. A. *Surf. Sci.* **1997**, *380*, 302.
(64) Cruz, C. D. L.; Sheppard, N. *J. Chem. Soc., Faraday Trans.* **1997**, *93*, 3569.
(65) Moshin, S. B.; Trenary, M.; Robota, H. J. *J. Phys. Chem.* **1991**, *95*, 6657.
(66) Beebe, J. T. P.; Yates, J. J. T. *Surf. Sci.* **1986**, *173*, L606.
(67) Paul, D. K.; Beebe, T. P.; Uram, K. J.; Yates, J. T. *J. Am. Chem. Soc.* **1992**, *114*, 1949.
(68) Crooks, R. M.; Zhao, M.; Sun, L.; Chechik, V.; Yeung, L. K. *Acc. Chem. Res.* **2001**, *34*, 181.
(69) Narayanan, R.; El-Sayed, M. A. *J. Phys. Chem. B* **2005**, *109*, 12663.
(70) Ott, L. S.; Finke, R. G. *Inorg. Chem.* **2006**, *45*, 8382.
(71) Pérez-Dieste, V.; Castellini, O. M.; Crain, J. N.; Eriksson, M. A.; Kirakosian, A.; Lin, J.-L.; McChesney, J. L.; Himpsel, F. J.; Black, C. T.; Murray, C. B. *Appl. Phys. Lett.* **2003**, *83*, 5053.
(72) Wang, Y.; Zhang, J.; Wang, X.; Ren, J.; Zuo, B.; Tang, Y. *Top. Catal.* **2005**, *35*, 35.
(73) Kim, F.; Connor, S.; Song, H.; Kuykendall, T.; Yang, P. *Angew. Chem., Int. Ed.* **2004**, *43*, 3673.
(74) Garcia-Gutierrez, D. I.; Gutierrez-Wing, C. E.; Giovanetti, L.; Rampallo-López, J. M.; Requejo, F. G.; Jose-Yacaman, M. *J. Phys. Chem. B* **2005**, *109*, 3813.
(75) Borodko, Y.; Habas, S. E.; Koebel, M.; Yang, P.; Frei, H.; Somorjai, G. A. *J. Phys. Chem. B* **2006**, *110*, 23052.
(76) McDermott, D. P. *J. Phys. Chem.* **1986**, *90*, 2569.
(77) Bonet, F.; Tekaia-Elhsissen, K.; Sarathy, K. V. *Bull. Mater. Sci.* **2000**, *23*, 165.
(78) Gao, Y.; Jiang, P.; Liu, D. F.; Yuan, H. J.; Yan, X. Q.; Zhou, Z. P.; Wang, J. X.; Song, L.; Liu, L. F.; Zhou, W. Y.; Wang, G.; Wang, C. Y.; Xie, S. S.; Zhang, J. M.; Shen, D. Y. *J. Phys. Chem. B* **2004**, *108*, 12877.
(79) Zhang, Z.; Zhao, B.; Hu, L. *J. Solid State Chem.* **1996**, *121*, 105.
(80) Peek, P. S.; McDermott, D. P. *Spectrochim. Acta, Part A* **1988**, *44*, 371.
(81) Du, Y. K.; Yang, P.; Mou, Z. G.; Hua, N. P.; Jiang, L. *J. Appl. Polym. Sci.* **2006**, *99*, 23.
(82) Kawai, T.; Neivandt, D. J.; Davies, P. B. *J. Am. Chem. Soc.* **2000**, *122*, 12031.
(83) Borodko, Y.; Humphrey, S. M.; Tilley, T. D.; Frei, H.; Somorjai, G. A. *J. Phys. Chem. C* **2007**, *111*, 6288.
(84) Deutsch, D. S.; Lafaye, G.; Liu, D.; Chandler, B.; Williams, C. T.; Amiridis, M. D. *Catal. Lett.* **2004**, *97*, 139.
(85) Kuhn, J. N.; Tsung, C. K.; Huang, W.; Somorjai, G. A. *J. Catal.* **2009**, *265*, 209.
(86) Park, J. Y.; Aliaga, C.; Renzas, J. R.; Lee, H.; Somorjai, G. A. *Catal. Lett.* **2009**, *129*, 1.
(87) deCaro, D.; Köhler, J.; Busser, W.; Bradley, J. *Macromol. Symp.* **2000**, *156*, 53.
(88) Aliaga, C.; Park, J. Y.; Yamada, Y.; Lee, H. S.; Tsung, C. K.; Yang, P. D.; Somorjai, G. A. *J. Phys. Chem. C* **2009**, *113*, 6150.
(89) Crespo-Quesada, M.; Andanson, J. M.; Yarulin, A.; Lim, B.; Xia, Y. N.; Kiwi-Minsker, L. *Langmuir* **2011**, *27*, 7909.
(90) Krier, J. M.; Michalak, W. D.; Baker, L. R.; An, K.; Komvopoulos, K.; Somorjai, G. A. *J. Phys. Chem. C* **2012**, *116*, 17540.